PHYS2041/2941/7141 Lab Report 1

Samuel Allpass s4803050
School of Mathematics and Physics, University of Queensland, Brisbane, QLD 4072, Australia

This investigation aimed at quantitatively expressing the accuracy of the hydrogen Bohr model when calculating the energy levels for atoms with one valence electron, specifically sodium. It was hypothesised that the Bohr model could be rectified to account for lower orbiting electron potentials by subtracting from the principle quantum number by some quantum defect δ_l. A spectrometer was calibrated using a mercury lamp to first determine a linear regression between the measured angles of refraction against theoretically accepted wavelengths of mercury's emission spectrum. This regression was then utilised to determine the wavelengths of sodiums emission spectrum and further its orbitals energies. Given such data, it was found that subtracting from the principle quantum number by the quantum defects (1.2 ± 0.4), (0.7 ± 0.2) and (2 ± 1) for s, p and d respectively accurately predicted the energies of such orbitals, thus, supporting the hypothesis. However, the experimental quantum defects proved deviant to the currently accepted values of 1.35, 0.86 and 0.01 for s, p and d respectively [1]. Thus, it was recommended that future experiments utilise a digital Vernier scale and a larger number of trials to instill higher confidence in the resulting quantum defects.

I. INTRODUCTION

For over a century quantum mechanics has pioneered modern physics. In 1913 Niels Bohr proposed the current Bohr model, detailing the structure of the hydrogen atom as well as the distinct energy values for its electron orbitals [2]. In testing the Bohr model, this investigation proceeded to calculate experimental values for the energy of an sodium's single valence electron in excited states in order to judge the Bohr models accuracy in predicting the energy levels of other hydrogen-like atoms. It was aimed that quantised values can be calculated to rectify the Bohr model and its neglected quantum complexities. The reports findings will provide a clear basis for future physics research, such that the appropriateness of using the Bohr model in a given situation can be evaluated.

II. THEORY

Atomic spectroscopy forever changed our understanding of quantum mechanics, posing a new method of determining specific elements within a sample. In 1666, Sir Isaac Newton first demonstrated that light could be separated into a continuous spectrum of colour through an apparatus such as a glass prism or lens. Demonstrated in figure 1, as a single ray of light passes through varying mediums, it is refracted. This refraction was quantised by Dutch Astronomer Willebrord Snell in 1621 given by Snell's Law [3]:

$$n_1 sin(\theta_1) = n_2 sin(\theta_2)$$

Where n reflects the mediums refractive index and θ the angle between the surfaces normal and the light ray.

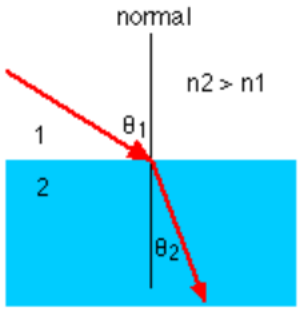

FIG. 1. Diagram depicting refraction of light from medium 1 to 2. Highlights elements in order to solve Snell's law [4].

Interestingly, the refractive index itself depends on the wavelength of the light ray. As a result, each wavelength of light is refracted to a different extent given the mediums and angles of incident remain the same. For white light, this accounts for the continuous spectrum observed by Newton and is depicted in figure 2.

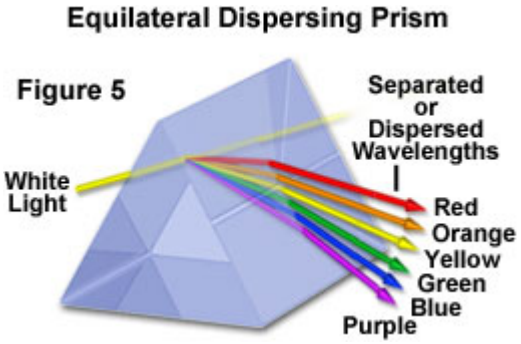

FIG. 2. Diagram depicting refraction of varying wavelengths of light through a prism [5].

Physicists began using this effect to investigate the wavelengths of an atoms emission spectrum through a

spectroscope [6]. As constructed in figure 3, a simple spectroscope consists of two scopes placed around a central prism, which as previously discussed has the purpose of separating some mixed light into into its superimposed wavelengths. The first scope contains a thin slit through which the source light emits. The wave-like nature of light causes the lights to disperse in different directions down the scope as if it were a point source. To rectify this, a collimating lens is positioned in the scope to adjust all the light rays into parallel, such that they all have the same angle of incident compared to the normal of the prism. After passing through the prism, the refracted light is then transferred through a focusing lens to which separates all the wavelengths into their positions on the spectral image plane.

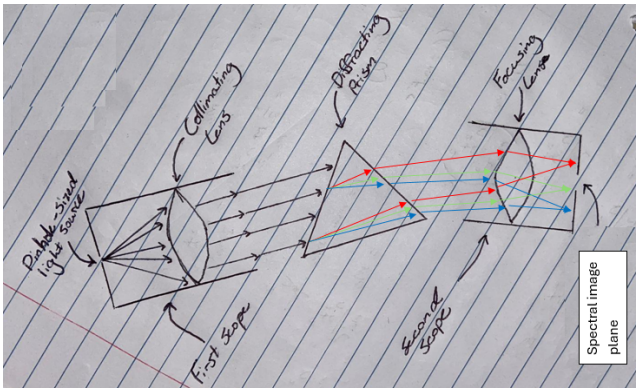

FIG. 3. Diagram depicting optical paths of different wavelengths of light through spectroscope.

In 1859, German phsicist Gustav Kirchoff and Chemist Robert Wilhelm Bunsen realised that the spectral lines emitted from each element were unique, such that the photons emitted by exciting the gaseous state of an element were equivalent in energy to the energy difference of two orbitals an electron could jump between. Using hydrogen as an example, an elements "fingerprint" emission spectrum appears on the spectral image plane as shown in figure 4.

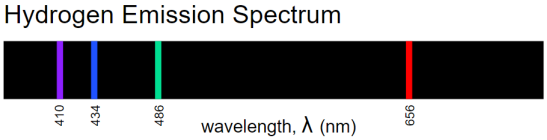

FIG. 4. Diagram depicting the spectroscopes spectral image plane, emission spectrum, for hydrogen [7].

After two centuries of appending to the periodic table with this breakthrough, Swedish physicist Johannes Rydberg simplified the Balmer series for hydrogen, found just three year prior by the Swiss physicist Johann Balmer in 1885. The Balmer-Rydberg series quantised the frequency of a photon emitted from an electrons de-excitement from some energy level n to m.

$$\nu = \frac{1}{\lambda} = Rc\left(\frac{1}{m^2} - \frac{1}{n^2}\right)$$

Where R is the Rydberg constant and c is the speed of light. Further to this postulate, Niels Bohr proposed the Nobel Prize winning theory of the Bohr model, such that the atom is comprised of a central mass nucleus of protons and neutrons orbited by electrons that can only occupy quantised energy levels. The Bohr model stood to validate the Balmer-Rydberg series for the simple case of the hydrogen atom. More specifically, the model highlighted four governing principles [8]; electrons occupy particular stable regions of space around the nucleus called "stationary" orbits; each stationary orbit has its own associated energy; the process of an electron jumping from an excited state to lower energy orbital will release a photon, and finally the energy of such a photon will follow:

$$\Delta E_{\text{light}} = E_F - E_I$$

Where E_F and E_I are the energies of the final and initial orbitals respectively. The model details that in the same way that force decreases by an inverse squared ratio, so to does the energy of each orbital, formally we can prove this using classical mechanics:

Treating an orbiting electron with classical centripetal motion and a charged particle, we find:

$$F_c = \frac{m_e v^2}{r_n} \quad and \quad F_c = \frac{q_1 q_2}{4\pi\epsilon_0 r^2} = \frac{Ze(-e)}{4\pi\epsilon_0 (r_n)^2}$$

Equating the two:

$$\frac{m_e v^2}{r_n} = \frac{Ze^2}{4\pi\epsilon_0 r_n^2} \quad equivalently \quad v^2 = \frac{Ze^2}{4\pi\epsilon_0 r_n m_e}$$

For an electron of angular momentum $n\hbar$ it is understood that:

$$L = n\hbar = m_e v r_n \quad such\ that \quad v = \frac{n\hbar}{m_e r_n}$$

And so follows:

$$v^2 = \frac{Ze^2}{4\pi\epsilon_0 r_n m_e} = (\frac{n\hbar}{m_e r_n})^2 \quad or \quad r_n = \frac{n^2\hbar^2}{4\pi\epsilon_0 m_e e^2}$$

To finalise the derivation, Virials theorem is applied to find the total energy of an electron in the $n-1^{th}$ excited state:

$$E_n = U + K = U + \frac{U}{2} = \frac{-e^2}{4\pi\epsilon_0 r_n} + \frac{-e^2}{2 * 4\pi\epsilon_0 r_n}$$

Which when r_n is substituted in from above, and the

reduced mass μ is substituted for the general case:

$$E_n = -\frac{\mu Z^2 e^4}{2(4\pi\epsilon_0)^2\hbar^2}\frac{1}{n^2}$$

Thus, the equation derived quantised the energy of the n^{th} principle quantum number for hydrogen and clearly demonstrated the inverse squared relationship between energy and n. This is visually demonstrated by hydrogens energy level Grotrian diagram in figure 5.

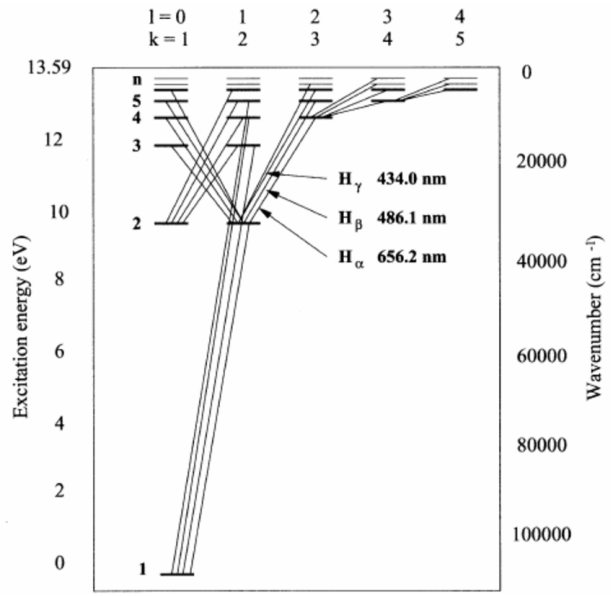

FIG. 5. Grotrian energy level diagram for hydrogen [9].

It was reasoned that this inverse relationship is conserved for any potential acting on an electron, such that altering Z accordingly would only change the magnitude of the energy levels. Modern quantum physics outlines that the energy of any particle can be determined by:

$$(\frac{\hbar}{2\mu}\nabla^2 + V)\Psi = E\Psi$$

For a purely coulomb potential, the principle quantum number is restricted to positive integers greater than 0 in order to satisfy the time independent Schrödinger equation. Further to this quantisation, detailed investigations into the more general Schrödinger equation reveal E to also be dependent on a second variable l, the electrons angular momentum state, which in the quantised coulomb case becomes confined to integers from 0 to (n-1). By convention, we notate the orbital angular momentum's 0, 1 and 2 to be s, p and d respectively. Additionally, further analysis reveals the existence of two more values, the magnetic quantum number, confined to values between -l and l, and the electrons intrinsic spin, $\pm 1/2$. Although these two variables are not of interest in this report, it is important to recognise that no two electrons can be identical in all four quantum variables. As such, the orbitals are filled in a particular configuration, with the s, p and d orbitals having capacities of 2, 6 and 10 electrons each purely based on the permutations of the four quantum variables. Whilst hydrogen presented a scenario containing a simple coulomb potential with an electron configuration $1s^1$, it was hypothesised that for other Alkali atoms, elements with only one valence electron but differing electron configurations, the Bohr model would pose limitations. It was suggested that quantum effects such as electron shielding, the reduction in nuclei potential V experienced by the valence electron due to the presence of intermediary electrons, would reduce the accuracy of the Bohr model energies [10]. It was discussed that an adjusted general solution to E_n could be identified by adjusting the principle quantum number by some quantum defect:

$$E_n = -\frac{A}{(n-\delta_l)^2} \quad \textit{or equivalently} \quad \frac{1}{\sqrt{-E}} = \frac{1}{\sqrt{A}}n - \frac{\delta_l}{\sqrt{A}}$$

Where δ_l is a quantum defect for the angular momentum's s, p or d. It is crucial to understand that the quantum defect was hypothesised to differ for s, p and d as the varying orbital positions in space would effect potential, and further the orbital energy. Given this general form for any alkali metal, the linear plot of measured values for E and n would result in a plot through which A and δ_l could be extracted from the gradient and y-intercept respectively.

The investigated alkali metal sodium has an electron configuration $1s^1 2s^2 2p^6 3s^1$. From this it was observed that the valence electron for sodium occupies a higher energy level than that of hydrogen, as such, the investigation would only analyse the energy levels above and including 3s. Additionally the investigation relied upon theoretically accepted wavelengths of the mercury emission spectrum given in table 1, and that the 3s orbital for sodium had an energy -5.139eV below the ionisation limit.

Wavelength (nm)	**Colour**
404.655	violet
407.781	violet
435.835	blue
491.604	blue/green
546.074	green (bright)
576.959	yellow
579.065	yellow

TABLE I. Wavelengths and corresponding colours of the mercury emission spectrum.

III. METHOD

A. Uncertainties

In order to minimise the uncertainty of the final results, it was first observed that there were three locations of uncertainty. The first was outlined in our measurements for the angle of refraction. The spectroscope used consistently through the experiment was situated with a Vernier scale as shown in figure 6. The top of the Vernier scale measured on the scale of 1^o, however, the bottom was utilised to append two decimal points to the measurement. As such, it was reasonably concluded that all angle measurements should contain a purely instrumental uncertainty of $\pm 0.005^o$, such that it is half the smallest increment of measurement. Secondly, as demonstrated in figure 6, the spectroscope relied on the accurate placement of a cross-hair on top of the spectral lines in order to measure the angle. Although confident in our cross-hair placement and ability to read the Vernier scale, it was justified that any angle measurement should result in a $\pm 0.5^o$ uncertainty. Specifically, this value was chosen as seemingly small adjustments to the cross-hair, such that they still lay within the observable bounds of the diffracted line caused our result to vary by this amount. To conclude our angle uncertainty, considering the Vernier uncertainty was negligible in comparison to human error, our measured angles would attain an uncertainty of $\pm 0.5^o$. Finally, given that any uncertainty in the theoretical data retrieved in the previous theory section would similarly be negligible compared to human error, the investigation would not propagate any uncertainties in such values.

B. Apparatus

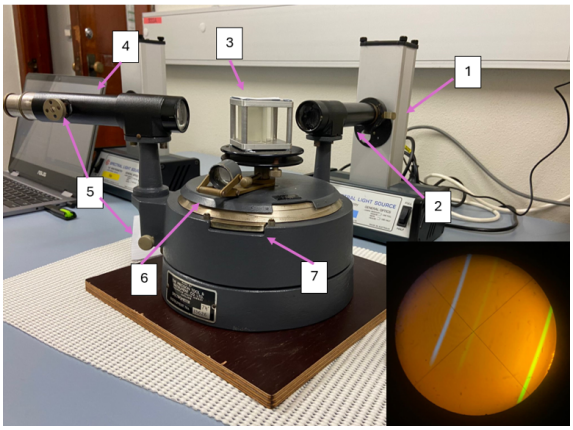

FIG. 6. Diagram depicting the experimental setup of the spectrometer in addition to light source. Labels 1-7 discussed below.

In a similar fashion to the spectrometer previously discussed, the apparatus consisted of a sodium spectral light source (1) with a small slit opening. The source was placed in front of the first scope (2) which as detailed above used a collimating lens to focus parallel rays of light down to the prism (3). Not only did the source already slim the light through a slit, a secondary dial on the first scope allowed for the amount of light passing through to be controlled. The prism was positioned as to refract each wavelength of light towards the second scope (4) which refocused the wavelengths through a focusing lens onto a spectral image plane. Further to this basic functionality however, the second scope was also equipped with positional controls (5), such that a top dial slid a lens to adjust the focal length for viewing purposes whilst lower dials horizontally shifted the entire scope precisely. It is this precise movement that caused the Vernier scale to shift (7), such that angle values could be carefully examined using the magnifying glass (6).

C. Procedure

In order to commence with the experiment, a setup procedure was conducted in order to correctly record refraction angle measurements for given wavelengths of sodium. First came a calibration stage in which a mercury lamp source was used. This section had two purposes, first to ensure that the refracted light made its way correctly down to the spectral image plane, and secondly to create an initial linear regression between the theoretically accepted wavelengths of mercury's emission spectrum and the angle at which they were refracted. This procedure was conducted as follows. First the mercury lamp was turned on and allowed to heat, shining through its small slit opening. The opening was then positioned to shine down the first scope such that it traveled down to the prism. Whilst maintaining the prism a constant angle, a piece of paper was revolved around the prism to track down the refracted light rays. Once found, the second scope could then be re-positioned to line up with the refracted light rays. Whilst this basic setup is complete, it is unlikely that the spectral lines would appear discrete and clear. To rectify this, the first scopes knob was adjusted to vary the amount of light passing through the spectrometer, and the second scopes knob was adjusted to shift the focal point to the observing pinhole. It is important to note that adjusting these dials could be done at any time throughout the experiment to improve accuracy for specific trials without affecting the resulting linear regression. From this position, using the dials located below the lens, the observer could finely align the center of the cross-hair with the spectral lines. With the cross-hair aligned, the magnifying glass could then be used to observe the angle measured on the Vernier scale. This measurement process was repeated for all the spec-

tral lines observed, ensuring that the lamp, first scope and prism were all maintained in a constant position. It was suggested that the spectral lines be recorded from one end of the spectrum to the other to ensure none were missed or incorrectly identified as other expected wavelengths.

With mercury angles recorded, the lamp could then be substituted for the sodium lamp, ensuring that scope one and the prism were kept stationary. Completing the same process of measurement for sodium, the resulting angles could be modelled against the linear regression between wavelength and angle found in the mercury calibration stage, such as to calculate values for the wavelengths found in sodium's emission spectrum. However, it is crucial to understand that if trials were to be repeated on different days or varying equipment, the calibration stage with mercury would have to be replicated in order to form a new relevant linear regression.

In the conducted experiment, to reduce uncertainty in the wavelengths calculated for sodium, it was reasoned that three trials would be conducted over two separate periods separated by a week, one trial initially, two in the following week. This ensured that by taking the average of the three trials, the wavelengths for sodium's emission spectrum would be of higher accuracy.

IV. RESULTS

After conducting the calibration method outlined previously, the data produced the linear relationship between the known wavelength of mercury's emission spectrum from table 1, and the measured angle of refraction. This was shown in figure 7 and 8. The calibrations were handled to include $\pm 0.5^o$ of uncertainty and was propagated into the linear regression appropriately using a Java-Matlab software.

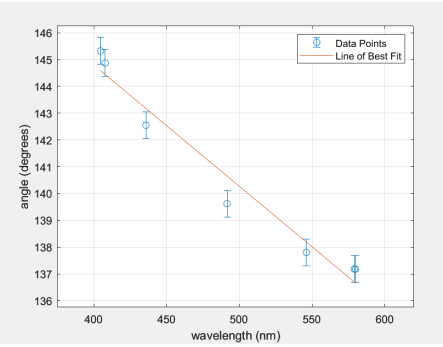

FIG. 7. Results for first conducted mercury calibration. Regression given by equation: $\theta = (-0.0452 \pm 0.0040)\lambda + (162.8702 \pm 1.9499)$

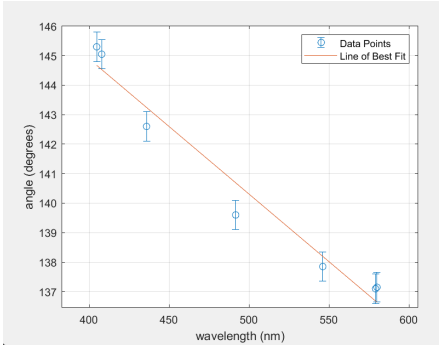

FIG. 8. Results for second conducted mercury calibration. Regression given by: $\theta = (-0.0458 \pm 0.0039)\lambda + (163.2040 \pm 1.9438)$

Although the linear regressions could be analysed to explain and justify some theoretical relationship between wavelength and angle of refraction, for example Snell's law, it was concluded that such an activity would be meaningless in the final conclusion of the investigation. However, simply observing Snell's law, it becomes apparent that wavelength and angle of refraction share a sinusoidal relationship. However, considering that all angles of refraction fall within a small domain, it was concluded that the small angle approximation justified the use of a linear regression.

Following the second section of the method, the same process was conducted for sodium. Given the linear regression previously discovered, the wavelengths of sodium's emission spectrum were calculated given for the measured angles as follows:

$$\lambda = \frac{\theta - c}{m}$$

Following this, the uncertainty was propagated accordingly:

$$\sigma_\lambda^2 = (\frac{\delta\lambda}{\delta m})^2\sigma_m^2 + (\frac{\delta\lambda}{\delta c})^2\sigma_c^2 = (ln|\theta - c|)^2\sigma_m^2 + (\frac{1}{-m})^2\sigma_c^2$$

The wavelengths for each trial were calculated using their respective calibration regressions, and further an average was taken as shown in appendix A. This average was displayed in table 2 and was calculated as follows.

$$\lambda_{average} = \frac{\sum_{i=1}^{n}\lambda_i}{n} \; \Delta\lambda_{average} = \frac{\sqrt{(\Delta\lambda_1)^2 + ... + (\Delta\lambda_n)^2}}{n}$$

It is also important to note that the infrared and ultraviolet colours were given by theoretically accepted values and therefore no reasonable uncertainty could be assigned. Further to this, it was understood that the relationship:

$$E = \frac{hc}{\lambda} * 6.242 * 10^{18} \; \Delta E = E_\lambda\sqrt{(\frac{\Delta\lambda}{\lambda})^2}$$

where h is Plank's constant and c is the speed of light could be used to calculate the energy, in electron volts, of a photon of wavelength λ.

Colour	Orbital transition	Wavelength (nm)	Energy (eV)
infrared	4s -> 3p	1139 ± 0	1.1 ± 0
infrared	3d -> 3p	819 ± 0	1.5 ± 0
red	5s -> 3p	590 ± 20	2.10 ± 0.09
yellow (bright)	4p -> 3s	570 ± 20	2.17 ± 0.09
green	3p -> 3s	560 ± 20	2.22 ± 0.09
green	4d -> 3p	530 ± 20	2.3 ± 0.1
green	6s -> 3p	520 ± 20	2.4 ± 0.1
blue-green	5d -> 3p	450 ± 20	2.5 ± 0.1
blue	7s -> 3p	490 ± 20	2.5 ± 0.1
violet (weak)	6d -> 3p	470 ± 20	2.6 ± 0.1
violet (weak)	8s -> 3p	440 ± 20	2.8 ± 0.2
violet (weak)	7d -> 3p	430 ± 20	2.9 ± 0.2
violet (weak)	8d -> 3p	420 ± 20	2.9 ± 0.2
ultraviolet	9s -> 3p	330.2 ± 0	3.8 ± 0
ultraviolet	9d -> 3p	285.3 ± 0	4.3 ± 0
ultraviolet	4p -> 3s	268.0 ± 0	4.6 ± 0

TABLE II. Wavelengths, Orbital Transitions, and Energy values (eV) with uncertainties for different colours of sodium's emission spectrum.

Importantly, it became apparent that given the theoretically accepted value for the energy of sodium's 3s orbital was previously discussed to be -5.139eV, the energies of all other orbitals could be calculated as the sum of photon energies. With red as an example emission wavelength, it was understood that this it corresponded to an electron de-excitation from 5s orbital to 3p, such that:

$$E_{5s} = 3s + (3p- > 3s) + (5s- > 3p)$$

$$\Delta E_{5s} = \Delta(3p- > 3s) + \Delta(5s- > 3p)$$

Through this method, table 3 was constructed, in which the orbitals were segregated into their respective angular momentum's, s, p and d. In addition to this a Grotrian was constructed in figure 8 to visualise the energy levels of sodium's orbitals, such that a comparison could be drawn with respect to hydrogen's Grotian. Rather than the energy of the orbitals, for evaluations sake, the table displays the inverse square root of negative energy, a statistic that was previously discussed to clearly outline the trend over varying principle energy numbers. The trivially calculated values had corresponding uncertainties:

$$\Delta\frac{1}{\sqrt{-E}} = \frac{1}{\sqrt{-E}}\sqrt{(\frac{\Delta E}{E})^2}$$

Principle Quantum Number	s 1/sqrt(-E)	p 1/sqrt(-E)	d 1/sqrt(-E)
3	0.44 ± 0	0.60 ± 0.02	0.83 ± 0.04
4	0.70 ± 0.04	0.9 ± 0	1.15 ± 0.09
5	1.07 ± 0.09	1.1 ± 0	1.3 ± 0.1
6	1.3 ± 0.1	1.4 ± 0	1.5 ± 0.1
7	1.4 ± 0.1		2.4 ± 0.2
8	1.7 ± 0.1		3.1 ± 0.2
9	6.6 ± 0.4		

TABLE III. Separated energy orbitals for each principle quantum number with uncertainties (1/sqrt(-E) values for s, p, and d orbitals).

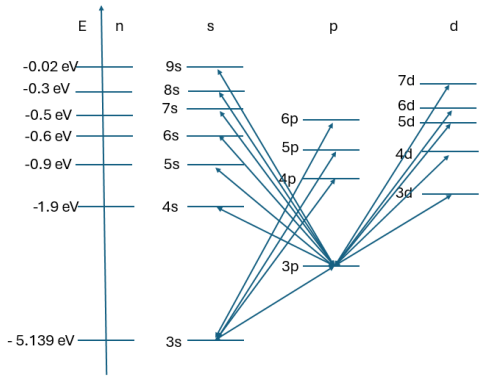

FIG. 9. Figure displays the experimentally calculated Grotrian for sodium.

Using the same Java-MATLAB linear regression previously encountered, figures 10, 11 and 12 were constructed to compare the relationship between the principle quantum number and the inverse root of the negative energy. In doing so, a quantised value for the quantum defect previously discussed could be reasonably calculated. The relationships found, with appropriate significant figures were as follows:

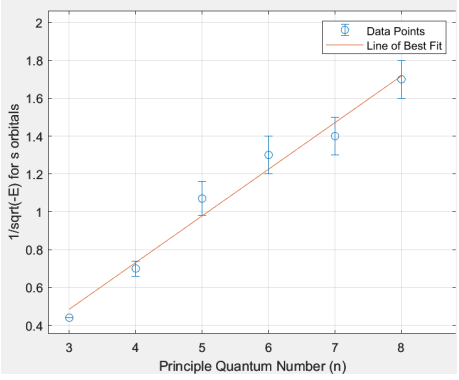

FIG. 10. Graph displays the relationship between principle quantum number and 1/sqrt(-E) for orbitals with angular momentum corresponding to s: $\frac{1}{\sqrt{-E}}$ = (0.25 ± 0.02)n + (-0.3 ± 0.1)

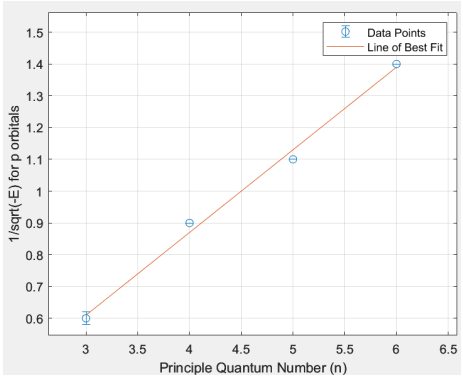

FIG. 11. Graph displays the relationship between principle quantum number and 1/sqrt(-E) for orbitals with angular momentum corresponding to p: $\frac{1}{\sqrt{-E}} = (0.26 \pm 0.01)n + (-0.17 \pm 0.06)$

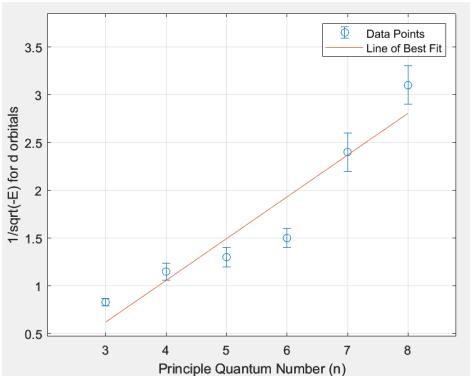

FIG. 12. Graph displays the relationship between principle quantum number and 1/sqrt(-E) for orbitals with angular momentum corresponding to d: $\frac{1}{\sqrt{-E}} = (0.44 \pm 0.07)n + (-0.7 \pm 0.4)$

Following this, given the adjusted Bohr model previously derived:

$$\frac{1}{\sqrt{-E}} = \frac{1}{\sqrt{A}}n - \frac{\delta_l}{\sqrt{A}}$$

It became apparent that the quantum defect for some l could be calculated as follows:

$$\delta_l = \frac{-c_l}{m_l} \quad and\ further \quad \Delta\delta_l = \delta_l\sqrt{(\frac{\Delta m_l}{m_l})^2 + (\frac{\Delta c_l}{c_l})^2}$$

And so following, the quantum defects for the s, p and d orbitals resulted as (1.2 ± 0.4), (0.7 ± 0.2) and (2 ± 1) with appropriate significant figures respectively.

It is important to note that the 9s orbital was excluded from calculations as it was found to significantly deviate from the trend expected trend and had an extremely large uncertainty. This exclusion was justified as the s orbitals already contained enough associated values in order to reasonably determine a trend.

Additionally, it was observed that the gradient of the graphs found correlates to the previously derived expression:

$$m_l = \sqrt{\frac{2(4\pi\epsilon_0)^2\hbar^2}{\mu Z^2 e^4}}$$

It was found that the reduced masses, μ, given by the s, p and d equations for sodium (Z=11) were $2.15 * 10^{-33}$, $2 * 10^{-33}$ and $6.95 * 10^{-34}$ kilograms respectively.

Qualitative trials were conducted to observe a high pressure sodium lamp over a period of time through the spectrometer. Figure 13 displays pictures of a high pressure sodium lamp over 0, 10 and 20 minutes respectively, the clear trend over which being that the spectrum broadens as time passes.

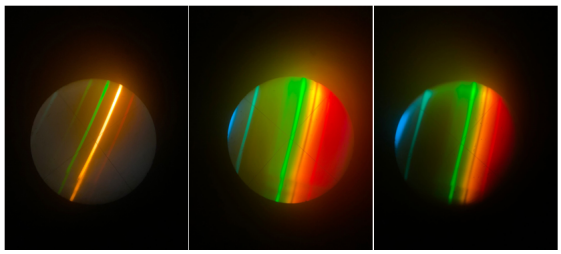

FIG. 13. Figure displays the spectral lines observed through the spectrometer of a high pressure sodium lamp over 0, 10 and 20 minutes.

V. DISCUSSION

When comparing the experimentally calculated Grotrian for sodium with that of hydrogen's, it becomes apparent that unlike hydrogen, the energies for sodium's oribtials for constant principle quantum numbers differ for s, p and d. This supports the hypothesis that the angular momentum will have an effect on the total energy due to the differences in potential for a given point in space. To quantise the translation found in the sodium Grotrian, it was found that a downshift to n of (1.2 ± 0.4), (0.7 ± 0.2) and (2 ± 1) for s, p and d respectively would account for the respective changes in potential.

The low pressure and high pressure sodium lamps had almost identical functionality. A potential difference from two electrodes is applied across a tube of sodium metal vapor such as to create electrical arcs [11]. It is these arcs that result from the excitement and subsequent de-excitement of sodium's valence electrons in the potential difference, releasing photons of predominantly yellow wavelengths. Significantly however, high pressure sodium lamps operate at either higher temperatures, smaller volume or a higher concentration of sodium vapor than the low pressure counterpart which theoretically results in the property of emission spectrum broadening, such that

yellow is no longer as dominant in the spectrum. This directly correlates to collision theory, such that as the pressure of the system is increased, the potential effects, V, of surrounding particles are more likely to effect the energy levels of an electron in an excited state. As a result, the amount of time an electron spends in an excited state decreases with its uncertainty following suit. As such, Heisenberg's uncertainty principle dictates that the uncertainty in the energy must therefore increase, and subsequently the same must happen for wavelength [12] [13]:

$$\Delta E \Delta t \approx h$$

As a result, the once distinct spectral lines begin to merge as time passes and the uncertainty in wavelength increases, in other words, the spectrum broadens. This was evidently supported by figure 13, such that over time a broadening in the emission spectrum was observed. This broadening was especially apparent for the two yellow frequencies, such allowing the pressure to build, the distinctness of the yellow lines fade and begin to broaden and blend towards each other.

The similarities between all three trials built confidence in the method, however, it was identified that the 9s orbital proved deviant to the otherwise linear trend. It was concluded that this could be a direct result of two errors discovered in the method, human precision of cross-hair placement over the center of the spectral line, and similarly, the human approximation of the Vernier scale readings. Although 9s proved a clear outlier to the trend, all other measurements carried clear justified uncertainties that account for this human inaccuracy. Similarly, in evaluating the experimental quantum defect values against the theoretical values, 1.35, 0.85 and 0.01 for s, p and d respectively, it is observed that δ_s and δ_p reflect the theoretically accepted values, however, δ_d differs dramatically [1]. It was hypothesised that this deviation from theory arose due to limited accurate data for the d angular momentum. Whilst the trends in the s and p orbitals reflect the theoretically accepted values, it was argued that the methodology was still flawed in its restricted number of trials, especially considering all but one of the p orbital energies were theoretical. Although no easily implementable solutions to error placing the cross-hair were reasoned, it was identified that two extensions to the method could be made to increase the accuracy of the final quantum defects calculated. Introducing a digital Vernier scale would dramatically reduce the $\pm 0.5^o$ human uncertainty which accounted for the majority of the investigations uncertainty. It is important to note that the chosen human uncertainty proved reasonable throughout the method as it reflected all team members confidence in appropriately measuring the angle whilst also accounting for cross-hair accuracy. Secondly, increasing the number of trials of the experiment would increase confidence in the final results, specifically it is recommended that the trials would be conducted over multiple calibration stages.

VI. CONCLUSION

The aim of the experiment was to quantitatively outline the limitations of the Bohr hydrogen model when attempting to analyse other atoms with one valence electron. It was shown that a quantum defect downshift to n of (1.2 ± 0.4), (0.7 ± 0.2) and (2 ± 1) for s, p and d respectively were experimentally sufficient in accounting for the shift in orbital energies for sodium. Supporting such findings, the Grotrian for sodium (figure 9) revealed that the angular momentum indeed had an effect on the total energy of the state, unlike for hydrogen where it was independent (figure 5). This was concluded to result from the differing potentials, V, experienced by electrons occupying different regions of space due to the varying angular momentum's. Further, it was also determined that the reduced mass deviated severely from the theoretically accepted $9.1 * 10^{-31}$kg, posing yet another limitation to the Bohr model. Additionally, it was shown that the emission spectrum for the higher pressure sodium lamp justifies the significance that potential altering particles inherently effect the energies of sodium's orbitals. Conclusively, the investigation supported current understandings in modern physics that the simplistic Bohr model proves inaccurate for atoms with lower orbiting electrons due to the changes in potential V. In the grand scheme, the results prove a basis for further investigations into the true quantitative expressions for more complex hydrogen-like atoms whilst also qunatising the reasonableness of using the Bohr model in future investigations.

[1] V. A. Kostelecky and M. M. Nieto, Analytical wavefunctions for atomic quantum-defect theory, Physical Review A **32**, 3007 (1985), received 12 August 1985.

[2] The nobel prize in physics 1922: Niels bohr (2024), accessed: 2024-09-07.

[3] E. Britannica, Snell's law (2024), accessed: 2024-09-06.

[4] B. University, Refraction (2024), accessed: 2024-09-06.

[5] F. S. University, Refraction of light (2024), accessed: 2024-09-06.

[6] U. Author, Timeline of atomic spectroscopy, https://www.spectroscopyonline.com/view/timeline-atomic-spectroscopy (2021), accessed: 2024-09-06.

[7] University of Texas at Austin, Hydrogen atom (2024), accessed: 2024-09-07.

[8] F. S. University, Quantum numbers and orbitals (2023), accessed: 2024-09-06.

[9] R. Tonelli and F. Meloni, Grotrian scheme relating the lines in the hydrogen spectrum to the atomic energy levels (2002), accessed: 2024-09-11.
[10] Unizin, Core and valence electrons, shielding, and zeff (m7q8), accessed: 2024-09-11.
[11] E. T. Center, Sodium lamps (2024), accessed: 2024-09-11.
[12] nmsu, Pressure broadening of spectral lines, accessed: 2024-09-11.
[13] J. B. Anderson, Line broadening by neutral perturbers, in *Light Scattering by Ice Crystals: Fundamentals and Applications*, International Geophysics, Vol. 84, edited by K. N. Liou (Academic Press, San Diego, CA, 2002) pp. 1–583.

Appendix A: Calculations for sodium emission spectrum wavelengths from measured angle

	Trial 1			
Colour	angle (degrees)	uncertainty (degrees)	wavelength (nm)	uncertainty (nm)
infrared	na	0.5	608.8744589	0
infrared	na	0.5	574.4588745	0
red	0.5	0.5	566.2337662	42.44104994
yellow (bright)	0.5	0.5	535.2813853	42.44104987
green	0.5	0.5	523.8095238	42.44104985
green	0.5	0.5	501.0822511	42.4410498
green	0.5	0.5	492.6406926	42.44104978
blue-green	0.5	0.5	475.5411255	42.44104974
blue	0.5	0.5	450.4329004	42.44104968
violet (weak)	0.5	0.5	438.961039	42.44104965
violet (weak)	0.5	0.5	428.7878788	42.44104962
violet (weak)	0.5	0.5	330.24	0
violet (weak)	0.5	0.5	285.28	0
ultraviolet	na	0.5	268.04	0
ultraviolet	na	0.5	0	0
ultraviolet	na	0.5	0	0

	Trial 2			
Colour	angle (degrees)	uncertainty (degrees)	wavelength (nm)	uncertainty (nm)
infrared	na	0.5	1139	0
infrared	na	0.5	819	0
red	135.24	0.5	608.8744589	42.44105002
yellow (bright)	136.83	0.5	574.4588745	42.44104995
green	137.21	0.5	566.2337662	42.44104994
green	138.64	0.5	535.2813853	42.44104987
green	139.17	0.5	523.8095238	42.44104985
blue-green	140.22	0.5	501.0822511	42.4410498
blue	140.61	0.5	492.6406926	42.44104978
violet (weak)	141.4	0.5	475.5411255	42.44104974
violet (weak)	142.56	0.5	450.4329004	42.44104968
violet (weak)	143.09	0.5	438.961039	42.44104965
violet (weak)	143.56	0.5	428.7878788	42.44104962
ultraviolet	na	0.5	330.24	0
ultraviolet	na	0.5	285.28	0
ultraviolet	na	0.5	268.04	0

	Trial 3			
Colour	angle (degrees)	uncertainty (degrees)	wavelength (nm)	uncertainty (nm)
infrared	na	0.5	1139	0
infrared	na	0.5	819	0
red	136.39	0.5	583.982684	42.44104997
yellow (bright)	136.86	0.5	573.8095238	42.44104995
green	137.31	0.5	564.0692641	42.44104993
green	138.69	0.5	534.1991342	42.44104987
green	139.28	0.5	521.4285714	42.44104984
blue-green	140.22	0.5	501.0822511	42.4410498
blue	140.65	0.5	491.7748918	42.44104977
violet (weak)	141.45	0.5	474.4588745	42.44104973
violet (weak)	142.58	0.5	450	42.44104968
violet (weak)	143.12	0.5	438.3116883	42.44104965
violet (weak)	143.65	0.5	426.8398268	42.44104962
ultraviolet	na	0.5	330.24	0
ultraviolet	na	0.5	285.28	0
ultraviolet	na	0.5	268.04	0

	Average of wavelengths				
Trial	1	2	3	Average Wavelength (nm)	Uncertainty in wavelength (nm)
infrared	1139	1139	1139	1139	0
infrared	819	819	819	819	0
red	580.3063457	608.8744589	583.982684	591.0544962	24.63847886
yellow (bright)	568.9277899	574.4588745	573.8095238	572.3987294	24.63847886
green	549.2341357	566.2337662	564.0692641	559.845722	24.63847884
green	527.1334792	535.2813853	534.1991342	532.2046662	24.63847881
green	513.1291028	523.8095238	521.4285714	519.4557327	24.63847879
blue-green	491.9037199	501.0822511	501.0822511	498.0227407	24.63847876
blue	481.4004376	492.6406926	491.7748918	488.6053407	24.63847875
violet (weak)	461.487965	475.5411255	474.4588745	470.4959883	24.63847873
violet (weak)	433.4792123	450.4329004	450	444.6373709	24.63847869
violet (weak)	421.0065646	438.961039	438.3116883	432.7597639	24.63847867
violet (weak)	406.7833698	428.7878788	426.8398268	420.8036918	24.63847866
ultraviolet	330.24	330.24	330.24	330.24	0
ultraviolet	285.28	285.28	285.28	285.28	0
ultraviolet	268.04	268.04	268.04	268.04	0

FIG. 14. Calculation of wavelength from raw angle values and average calculation table.